Research Square

Preprints are preliminary reports that have not undergone peer review.
They should not be considered conclusive, used to inform clinical practice,
or referenced by the media as validated information.

Microstructure and Mechanical Properties of Additively Manufactured Bimetallic TC4-8Cu Alloy/316 Stainless Steel

Xuanming Cui
Huazhong University of Science and Technology
Zhenghao Yin
Huazhong University of Science and Technology
Hui Du
Wuhan University of Science and Technology
Shengming Yin
yinsm@hust.edu.cn
Huazhong University of Science and Technology
Hebao Wu
Wuhan Institute of Technology
Jianguang Liu
COMAC Beijing Aircraft Technology Research Institute
Dongdong Li
Huazhong University of Science and Technology
Bing Ye
Wuhan Huagong Laser Engineering Co., Ltd
Shuren Guo
Huazhong University of Science and Technology
Xinwang Liu
Huazhong University of Science and Technology

Research Article

Keywords: Additive manufacturing, Electron beam powder bed fusion, Titanium/steel bimetallic structure, Interfacial reaction, Mechanical properties

Posted Date: November 20th, 2026

DOI: https://doi.org/10.21203/rs.3.rs-11595164/v1

License: This work is licensed under a Creative Commons Attribution 4.0 International License.
Read Full License

Additional Declarations: No competing interests reported.

Microstructure and Mechanical Properties of Additively Manufactured Bimetallic TC4-8Cu Alloy/316 Stainless Steel

Abstract

Titanium/steel bimetallic structures combine the high specific strength and excellent corrosion resistance of titanium alloys with the high ductility and low cost of stainless steels, offering broad application prospects in aerospace, nuclear energy, and marine engineering. However, direct joining is restricted by significant differences in their thermophysical properties and metallurgical compatibility, which readily lead to brittle Fe-Ti intermetallic phases and interfacial cracking. In this work, a TC4 alloy powder containing 8 wt.% Cu (TC4-8Cu) was used to fabricate a TC4-8Cu/316L bimetallic structure via electron beam powder bed fusion (EB-PBF). A metallurgically bonded, crack-free interface was obtained, consisting of the TC4-8Cu matrix, a Cu-rich zone, an intermetallic compound (IMC) layer, and the 316L matrix. Cu preferentially reacted with Ti to form Ti_2Cu near the interface, which consumed the available Ti, restricted Fe-Ti interdiffusion, and effectively suppressed the formation of continuous brittle Fe-Ti layers. Tensile tests revealed a distinct two-stage fracture process. At room temperature, the 316L side fractured first at a peak stress of 482 MPa, followed by load transfer to the titanium side, resulting in an ultimate tensile strength of 636 MPa. At 350 °C, the fracture sequence reversed: the TC4-8Cu side failed first at 618 MPa, and the remaining 316L section sustained a load-transfer stress of 190 MPa. These results demonstrate that powder-composition design with Cu can regulate interfacial reactions and preserve structural integrity in EB-PBF-fabricated titanium/steel bimetallic structures.

Keywords: Additive manufacturing; Electron beam powder bed fusion; Titanium/steel bimetallic structure; Interfacial reaction; Mechanical properties

1 Introduction

Titanium/steel bimetallic structures integrate the high specific strength and corrosion resistance of titanium alloys with the high ductility, structural capability, and relatively low cost of stainless steels. This combination offers considerable potential for aerospace, nuclear-energy, marine, and chemical-engineering applications in which different regions of a component are required to perform distinct structural or environmental functions [1-3]. However, the direct joining of titanium alloys and steels remains challenging because of their markedly different thermophysical properties and limited metallurgical compatibility. During fusion-based joining, mutual diffusion and chemical reactions between Ti and Fe can produce FeTi, Fe_2Ti, and other hard and brittle Fe-Ti intermetallic compounds at the interface [4, 5]. When these reaction products develop into a thick or continuous layer, the local mismatch in hardness and plastic deformation promotes stress concentration. This provides a preferential path for crack initiation and propagation. Therefore, it is crucial to control the interfacial reaction pathway and prevent the formation of a

continuous brittle Fe-Ti reaction layer while preserving effective load transfer across the interface.

Several processing strategies have been developed to mitigate these problems. Thermomechanical methods, such as rolling and forging, can disrupt surface films, increase the effective contact area, and promote bonding through the combined action of plastic deformation, pressure, and elevated temperature [6]. However, the interfacial thermal and deformation histories are strongly coupled, making it difficult to independently regulate heat input, elemental diffusion, and reaction-layer growth. In addition, conventional forming methods have limited geometric flexibility and commonly require extensive subsequent machining. Solid-state joining methods, including hot isostatic pressing diffusion bonding and explosive welding, can reduce bulk melting and thereby restrict the excessive formation of Fe-Ti intermetallic compounds [7]. Nevertheless, these methods generally require long processing times, specialized tooling and are therefore not readily applicable to the integrated manufacture of complex titanium/steel components. For instance, explosively welded Ti/Fe plates contain a brittle Fe_2Ti-dominated mixing zone where cracks readily form [8], and rotary friction welded TC4/316L joints exhibit an inhomogeneous interface along the radial direction [9].

Additive manufacturing provides an alternative route because it combines near-net shaping with localized energy input and spatially controlled material deposition [10-13]. In particular, electron beam powder bed fusion (EB-PBF) is suitable for processing reactive titanium alloys and for directly fabricating titanium/steel bimetallic structures due to its vacuum environment, high energy density,low residual stress, and controllable thermal input [14, 15]. However, the localized melting could promote metallurgical bonding as well as intensify the chemical interaction between Ti and Fe. Moreover, the thermal cycles due to layer-by-layer deposition may promote additional elemental diffusion and further growth of brittle reaction products. Consequently, process-parameter optimization alone may reduce interfacial defects, but it may not fundamentally alter the thermodynamic tendency for Fe-Ti intermetallic compounds to form. An additional material-design strategy is therefore required to redirect the interfacial reaction pathway.

One possible strategy is to introduce an alloying element that modifies elemental diffusion and competes with the direct reaction between Ti and Fe. For example, Ma et al. added 0.1 wt.% rare earth elements to a Ti-Zr-Cu-Ni-Co alloy, which promoted the uniform diffusion of Ti, Zr, Cu, Ni, and Co in the joint, increasing the joint tensile strength from 154 MPa to 204 MPa and the impact toughness by 50% [16]. These results indicate that regulating the chemical composition of the joining region can be as important as controlling the external processing parameters. Among different alloying elements, Cu is promising for regulating titanium/steel interfacial reactions.The Cu-Fe system is characterized by limited mutual solubility and the absence of stable intermetallic compounds [17], which reduces the likelihood of introducing an additional brittle compound layer on the steel side. In contrast, Cu can react with Ti to form Ti-Cu compounds, including Ti_2Cu and TiCu [18]. The

preferential participation of Cu in Ti-Cu reactions may consume part of the available Ti in the interfacial region and alter the diffusion and reaction sequence between Ti and Fe.

Cu interlayers have previously been used to improve titanium/steel joints [19, 20]. In an interlayer configuration, Cu is initially concentrated within a relatively narrow region between the two base materials.During welding, the Cu interlayer may melt almost completely, and its effectiveness in blocking Ti–Fe interdiffusion depends strongly on the interlayer thickness, local dissolution behavior, and diffusion distance. Moreover, even when Ti-Fe compounds are suppressed, the Ti-Cu compound layer can become the fracture site, as reported in electron beam welded Ti/Cu/Fe joints where the fracture occurred at the interfacial layer containing TiCu and Ti-Cu-Fe [21]. Directly incorporating Cu into the TC4 powder represents a fundamentally different material-design strategy. During EB-PBF, Cu is distributed throughout the titanium-side melt pool rather than being confined to the original joining plane. This broader distribution can simultaneously modify solidification of the deposited TC4 alloy, the supply of Cu to the interface, and the competitive formation of Ti-Cu and Fe-Ti reaction products [22, 23]. Such a powder-based approach also avoids the placement of a separate interlayer and is more compatible with layerwise fabrication of geometrically complex components. However, the resulting interfacial reaction products, transition-zone architecture, and mechanical consequences have not yet been sufficiently clarified. A systematic analysis combining microstructural observations, elemental distributions, phase identification, hardness measurements, and fracture behavior is required.

In addition to room-temperature performance, the response of the bimetallic structure at intermediate temperatures must be considered.TC4 titanium alloy and 316L stainless steel can both be used at approximately 350 °C, but their strength, ductility, and strain-hardening behavior change differently with temperature [24]. Consequently, the weakest region of a TC4-8Cu/316L bimetallic specimen may shift as the testing temperature increases. Clarifying the fracture sequence and post-fracture load transfer at 350 °C is therefore necessary for understanding the temperature-dependent mechanical response of the bimetallic structure.

Accordingly, in this study, a TC4-8Cu alloy containing 8 wt.% Cu was deposited directly onto a 316L stainless-steel substrate by EB-PBF. The interface was characterized using scanning electron microscopy, energy-dispersive X-ray spectroscopy, X-ray diffraction, and microhardness measurements, while the temperature-dependent load-bearing behavior was evaluated through tensile testing and fracture analysis. By correlating the interfacial reaction products with the fracture sequence and load-transfer behavior, this work aims to clarify the role of Cu in regulating the reaction pathway of additively manufactured titanium/steel interfaces and to evaluate the feasibility of powder-composition design as an alternative to conventional interlayer-based strategies.

2 Experimental

In this study, TC4-8Cu powder was prepared by high-energy ball milling of 92 wt.% TC4 powder and 8 wt.% pure Cu powder, followed by drying in a vacuum oven.

The powder particle size range was 45-150 μm. A 316L stainless steel plate was selected as the steel-side constituent of the bimetallic structure. TC4-8Cu powder was deposited on the 316L substrate by EB-PBF. The chemical compositions of the composite TC4-8Cu powder and the 316L stainless steel plate are listed in **Table 1** and **Table 2**, respectively.

Table 1 Chemical composition of composite TC4-8Cu powder (wt.%)

Element	Al	V	Fe	O	C	N	H	Si	Cu	Ti
Content	5.06	4.14	0.28	0.14	0.1	0.05	0.02	0.13	8	Bal.

Table 2 Chemical composition of 316L stainless steel substrate (wt.%)

Element	Si	Mn	S	P	C	Cr	Ni	Mo	Fe
Content	≤1	≤1	≤0.03	≤0.045	≤0.03	17	13	3	Bal.

Electron beam additive manufacturing was performed using a Y150 electron beam powder bed fusion (EB-PBF, Xi'an Sailong Additive Technology Co., Ltd) system consisted of an electron beam gun, a vacuum forming chamber, a powder spreading system, and a control system. Its main technical parameters are listed in

Table 3 After the vacuum level in the forming chamber was reduced below 2×10^{-1} Pa, the composite TC4-8Cu powder was directly deposited on the surface of the stainless steel plate. After the deposition of each layer, the substrate was heated to 900 °C via fast scanning. After deposition to the set height, the sample was allowed to cool to room temperature.

Table 3 Technical parameters of the electron beam additive manufacturing equipment

Parameter	**Value**
Rated power	3 kW
Scanning speed	5 m/s
Electron beam current	14 mA
Beam spot diameter	≤100 μm
Vacuum level	2×10^{-1} Pa
Preheating temperature	900 °C

Block specimens with dimensions of 4 mm × 2 mm × 2 mm were cut from the formed titanium/steel bimetallic structure sample for microstructural characterization. The sampling region covered the 316L stainless steel substrate, the interfacial transition layer, and the TC4 titanium alloy region, with the bonding interface positioned at the center of the observation surface. After grinding and polishing, the titanium alloy region and the stainless steel region were etched with Kroll's reagent (HF : HNO_3 : H_2O = 1 : 3 : 6 by volume) and aqua regia (concentrated HCl : concentrated HNO_3 = 3 : 1 by volume), respectively.

A Bruker D2 PHASER X-ray diffractometer (XRD) was used to analyze the phase composition of the interfacial region. A Gemini SEM 300 field-emission scanning electron microscope equipped with an energy-dispersive spectrometer (EDS) was used to observe the interfacial microstructure and perform micro-area elemental analysis.

Plate-shaped tensile specimens were cut from the interface of the titanium/steel bimetallic samples. Their shape and dimensions are shown in **Error! Reference source not found.** During sampling, the specimen axis was ensured to be consistent with the additive manufacturing deposition direction. The mechanical properties of the joints were tested using an AG-IC 100 kN electronic universal testing machine. The loading direction was parallel to the titanium/steel bonding interface to evaluate the overall load-bearing capacity and failure sequence of the bimetallic composite structure under loading parallel to the interface. A 430-SVD microhardness tester was used to measure the microhardness of the interfacial region. The measurement points were arranged continuously along the direction perpendicular to the interface from the titanium alloy side to the stainless steel side, with multiple rows measured at different height positions to characterize the interfacial hardness distribution.

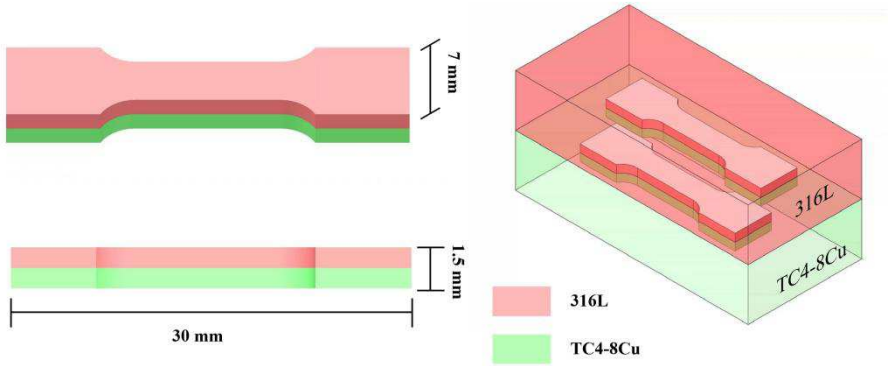

Fig. 1 Size of tensile specimen.

3 Results and discussion

3.1 Interfacial microstructure and phase constitution

The SEM morphology of the bonding interface of the EB-PBF fabricated TC4-8Cu/316L bimetallic structure is shown in **Error! Reference source not found.** The interface comprises the TC4-8Cu matrix, a multilayer reaction zone, and the 316L matrix. No through-thickness cracks were observed. The interface is wavy and distinct flow traces remain visible on the steel side, reflecting the electron-beam scanning path and melt-pool flow.

As shown in **Error! Reference source not found.a**, a dark-gray reaction layer is present near the titanium-side interface. Combined with the EDS mapping results in **Fig. 3** and **Fig. 4**, this region is enriched in Cu and thus identified as a Cu-rich zone. The point-scan results in **Table 4** further show that the Cu content at this region (Spot 2) is 2.72 at.%, higher than that in the other regions. This indicates that under electron beam thermal cycling, the added Cu underwent localized enrichment in the near-interface region on the titanium side.

Error! Reference source not found.b shows that the titanium matrix mainly consists of lamellar α phase and some intragranular acicular α phase, exhibiting a typical α+β duplex microstructure. Near the interface, the lamellae spacing is slightly larger compared to the central region of the deposited layer, which can be attributed to grain coarsening during multiple thermal cycles.

In **Error! Reference source not found.d**, the 316L matrix mainly exhibits austenitic microstructure characteristics while a small amount of gray-black vermicular phase is visible in the heat-affected zone near the interface, presumed to be δ-ferrite retained under rapid solidification condition.

Error! Reference source not found.c shows the high-magnification morphology of the interfacial region. The microstructure near the interface on the titanium side gradually transitions from fine equiaxed grains to coarse columnar grains, reflecting the complex thermal cycling and solidification processes experienced by the interfacial region during deposition. A small number of micron-scale pores are visible at the bonding interface and within the Cu-rich zone, which may be related to the Kirkendall effect caused by unbalanced interfacial elemental diffusion, that is, the diffusion rate of Ti toward the steel side is higher than that of Fe and Ni toward the titanium side, leading to vacancy accumulation and pore formation on the titanium side. In addition, the reaction of Cu with Ti to form Ti-Cu intermetallic compounds is accompanied by volume shrinkage, which may also exacerbate local stress concentration and promote pore nucleation [25]. The overall interfacial morphology and subsequent mechanical properties indicate that the positive effect of the Cu-rich zone in suppressing the continuous growth of Fe-Ti brittle phases is more significant.

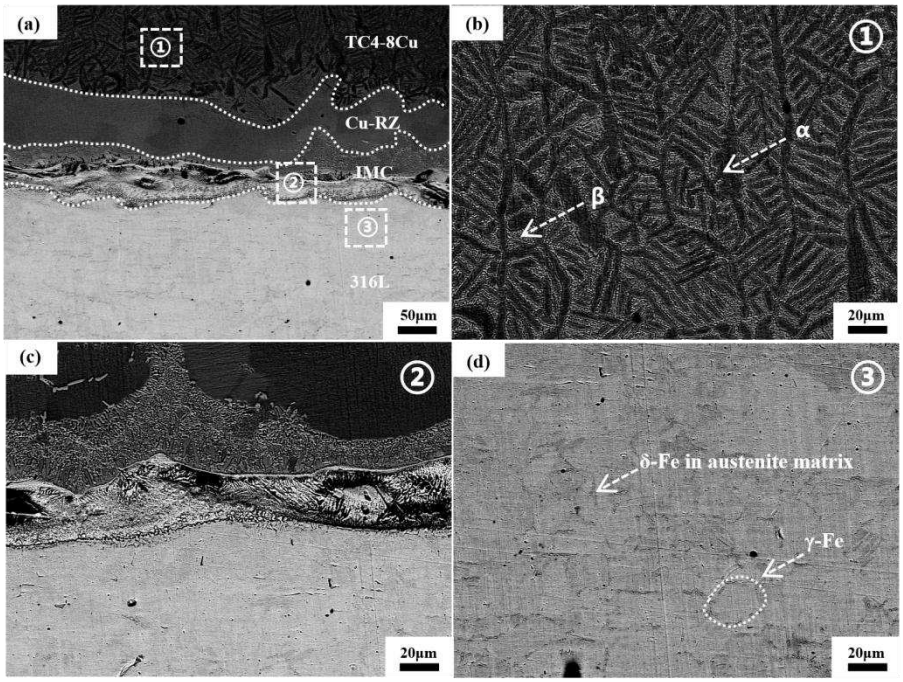

Fig. 2.SEM (BSE) microstructure morphology of the TC4-8Cu/316L interface. (a)Low-magnification morphology of the interface,showing the TC4-8Cu deposited layer, Cu-rich zone (Cu-RZ), intermetallic compound (IMC) zone, and 316L

substrate;(b)TC4-8Cu deposit;(c)High-magnification local morphology of the interface;(d) 316L substrate.

Fig. 3 and **Fig. 4** further reflect the elemental diffusion characteristics of the interfacial region. EDS mapping shows that Ti, Fe, Cr, Ni, and Cu all diffuse to a certain extent near the interface, but the elemental distribution on both sides of the interface still exhibits obvious gradient characteristics. Line scan results show that the concentration changes of Ti and Fe at the interface are relatively steep, indicating that their interdiffusion is insufficient due to rapid solidification. In contrast, Cu exhibits a distinct peak near the interface, further confirming that it mainly enriches in the Cu-rich zone and adjacent reaction zone, indicating that Cu does not simply diffuse across the interface but preferentially precipitates or participates in reactions in the near-interface region on the titanium side.

Combined with the point scan results in **Table 4**, the Ti/Fe atomic ratio at the interface region (point 3) is close to 2:1, which is attributed to local composition fluctuation or the transition region between Ti_2Cu and the Ti matrix, rather than the formation of a detectable Fe-Ti intermetallic compound, consistent with the XRD results below.

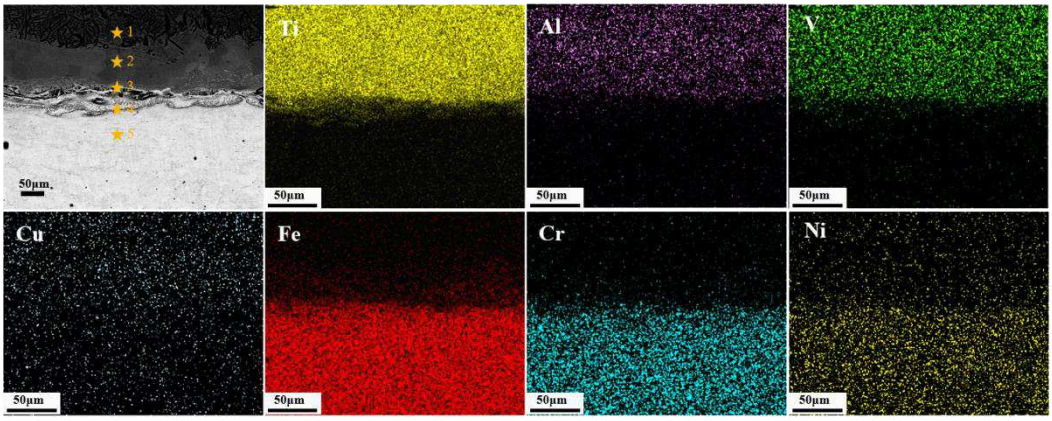

Fig. 3. EDS mapping results of the TC4-8Cu/316 stainless steel interface

Table 4 EDS point scan results of different regions in **Fig. 3.**（at.%）

Spot	Ti	Fe	Cr	Ni	Al	V	Cu
1	65.46	0.16	0.07	0.12	12.11	1.06	1.00
2	60.30	4.56	1.09	0.59	9.14	3.13	2.72
3	41.43	21.57	4.63	2.44	6.62	2.05	1.80
4	10.36	56.66	16.15	5.05	0.52	1.01	0.47
5	0.28	61.78	16.05	7.03	0.30	0.22	0.29

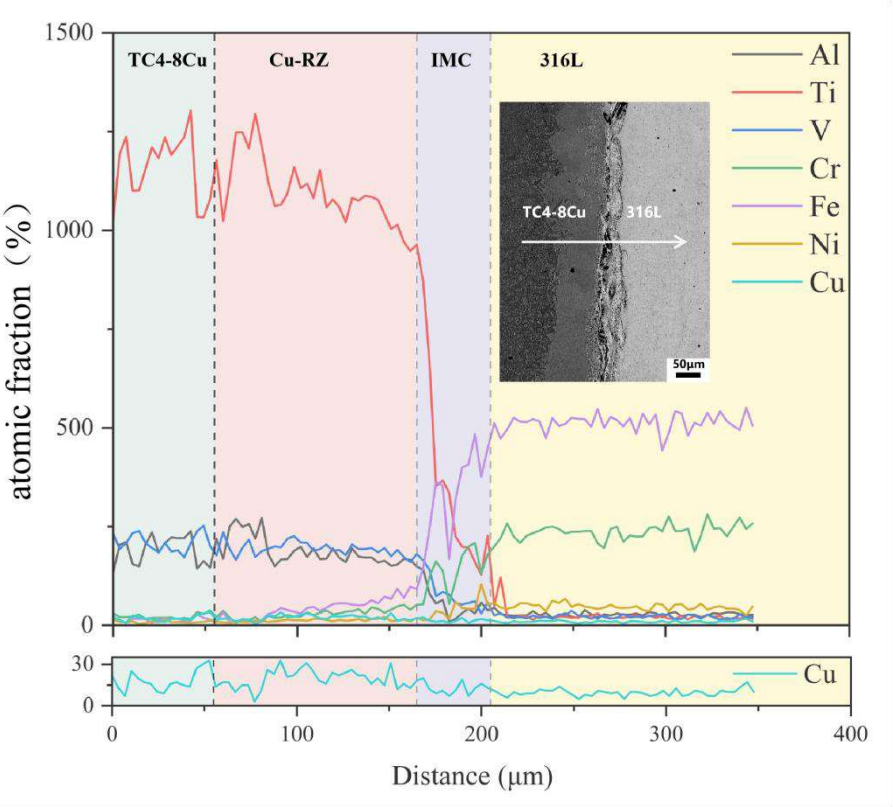

Fig. 4. EDS line scan results of the TC4-8Cu/316 stainless steel interface

To further clarify the interfacial phase composition,XRD analysis was performed on different regions of the bimetallic structure, as shown in **Fig. 5**. The deposited TC4-8Cu alloy mainly consists of α-Ti, β-Ti, and some Cu phase.The 316L substrate side mainly consists of austenite (γ-Fe) phase and δ-ferrite phase. The δ-ferrite is mainly distributed in the heat-affected zone near the interface. Ding et al. [26] also found a duplex microstructure of γ-austenite and δ-ferrite coexisting in electron beam additively manufactured 316L stainless steel and pointed out that δ-ferrite precipitates in interdendritic regions during rapid solidification. The δ-ferrite retained at some austenite grain boundaries is clearly visible under SEM, as shown in **Fig. 2d**. The phase composition of the interfacial region is the most complex. In addition to the α-Ti matrix phase, Ti_2Cu intermetallic compound was detected, while no obvious FeTi peak was observed. EDS line scan results show that significant concentration gradient changes of Fe and Ti near the interface, indicating that a certain degree of diffusion occurred between them at the interface. However, no obvious diffraction peaks of Fe-Ti intermetallic compounds appear in the XRD patterns. According to first-principles calculations and thermodynamic assessments of the Cu-Fe-Ti ternary system, the formation of Cu-Ti intermetallic compounds has a relatively high tendency than Fe-Ti compounds [27, 28], so that the available Ti in the melt was consumed by preferentially reaction with microalloying Cu instead of forming Fe-Ti phases. The illustration of element diffusion and interface compound formation is shown in **Fig. 6**. As a result, the TC4-8Cu/316L bonding interface ultimately forms a multilayer transition structure of TC4 matrix/Cu-rich zone/intermetallic compound zone/316L matrix, in which Cu changes the interfacial reaction path by preferentially

reacting with Ti to form Ti-Cu phases, suppressing the excessive growth of Fe-Ti brittle phases and preventing the formation of through-thickness brittle cracking channels.

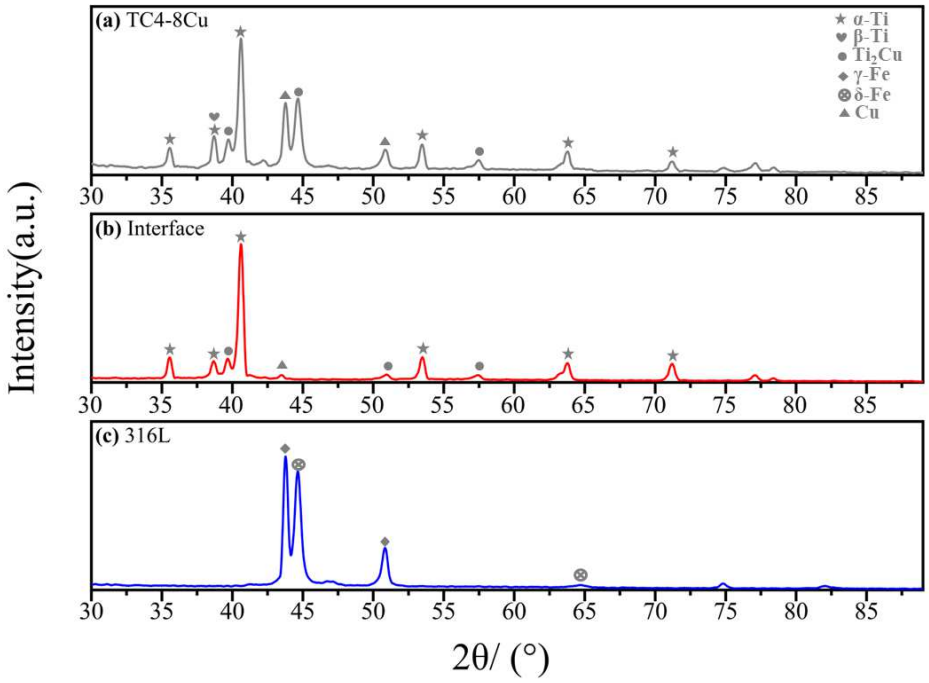

Fig. 5. XRD patterns of the TC4-8Cu/316 stainless steel interface at different positions

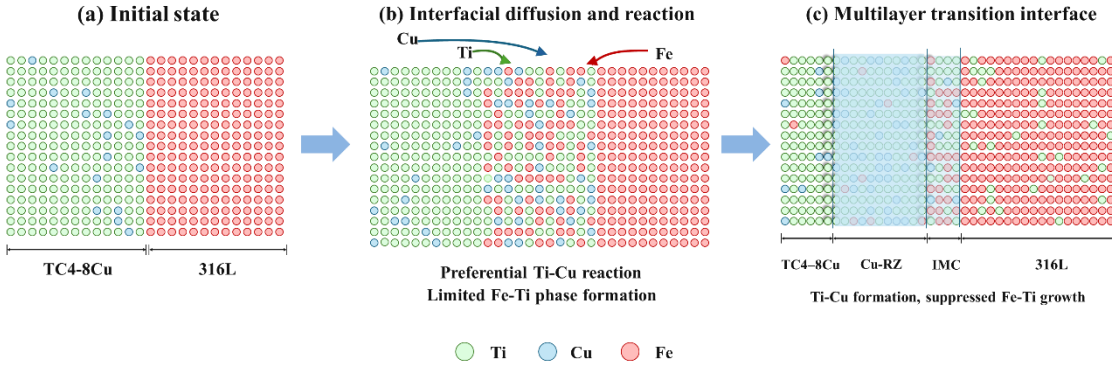

Fig. 6. Schematic of element diffusion and interface compound formation

3.2 Room-Temperature Tensile Properties and Hardness

Fig. 7 shows the room-temperature tensile stress-strain curves of the TC4-8Cu/316L bimetallic specimens, and Error! Unknown switch argument. lists the main mechanical property parameters. Combined with **Fig. 8**, the room-temperature tensile failure of the specimens exhibits a distinct two-stage fracture process characteristic. In the initial loading stage, both the titanium side and the steel side bear the load together. However, because the strength of 316L stainless steel is lower than that of the TC4-8Cu alloy, the steel side first reaches its limit and fractures. At this point, the interface has not completely failed, and the load can still be transferred to the titanium side through the metallurgically bonded interface, allowing the specimen to continue bearing load.

According to the stress–strain curve, point A corresponds to the first-stage peak stress, which is 482 MPa. This value reflects the maximum load that the interface can transfer before the steel side fractures, indirectly indicating the interfacial bonding strength. After the steel side completely fractures, the stress drops to point B, corresponding to a load-transfer stress of 252 MPa, after which the load is mainly borne by the titanium side. During continued loading, the titanium side undergoes plastic deformation and ultimately fractures, with an overall ultimate tensile strength of 636 MPa. In the tensile fracture morphology shown in **Fig. 8**, the steel side fracture exhibits no obvious necking, while the titanium side exhibits significant local deformation before fracture.Combined with the characteristic observed in the stress-strain curve that the load can still be transferred to the titanium side for continued bearing after steel-side fracture, the final failure mode at room temperature is that the steel side fractures first, followed by load transfer to the titanium side, and final fracture of the titanium side. This demonstrates that the interface possesses a certain load-transfer capability, ensuring continued load-bearing of the bimetallic structure after local failure.

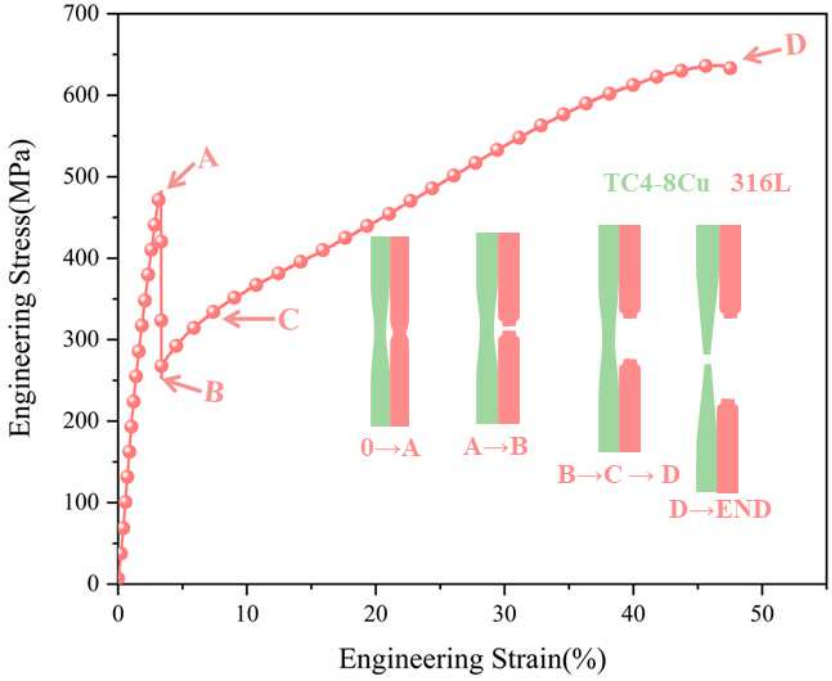

Fig. 7. Room-temperature tensile stress-strain curves of TC4-8Cu/316 stainless steel

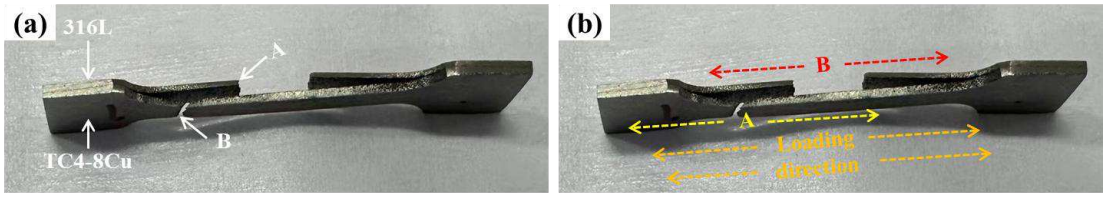

Fig. 8. Room-temperature tensile fracture morphology of TC4-8Cu/316 stainless steel

Table 5 Room-temperature mechanical property data

σ_1 (MPa)	σ_2 (MPa)	σ_b (MPa)	ε_1 (%)	δ (%)
482	252	636	3.3	47.1

σ_1=First-stage peak stress;σ_2=Load-transfer stress;σ_b=Ultimate tensile strength;ε_1=First-stage strain;δ=Total elongation at fracture.

Fig. 9 shows the microhardness distribution across the bonding interface. The measurement points extend from the TC4-8Cu deposited layer side across the interface to the 316L substrate side. Five data points were taken at each position and averaged, with the results listed in **Table 6** .The hardness of the titanium-side region is 419-435 HV, significantly higher than that of conventional annealed TC4 titanium alloy, mainly related to Cu solid-solution strengthening and the fine lamellar α + β and acicular α microstructure formed by rapid cooling during EB-PBF. The hardness of the Cu-rich zone increases to 495 HV, indicating that Cu enrichment and related precipitates play a significant role in local hardening. The intermetallic compound zone has the highest hardness, reaching 596-605 HV, which is presumed to be related to the presence of Ti-Cu intermetallic compounds. Overall, the interfacial hardness exhibits a gradient distribution, with high hardness on the titanium side, a peak at the interface, and low hardness on the steel side, indicating the presence of a mechanical property transition zone at the interface without the formation of a through-thickness brittle layer.

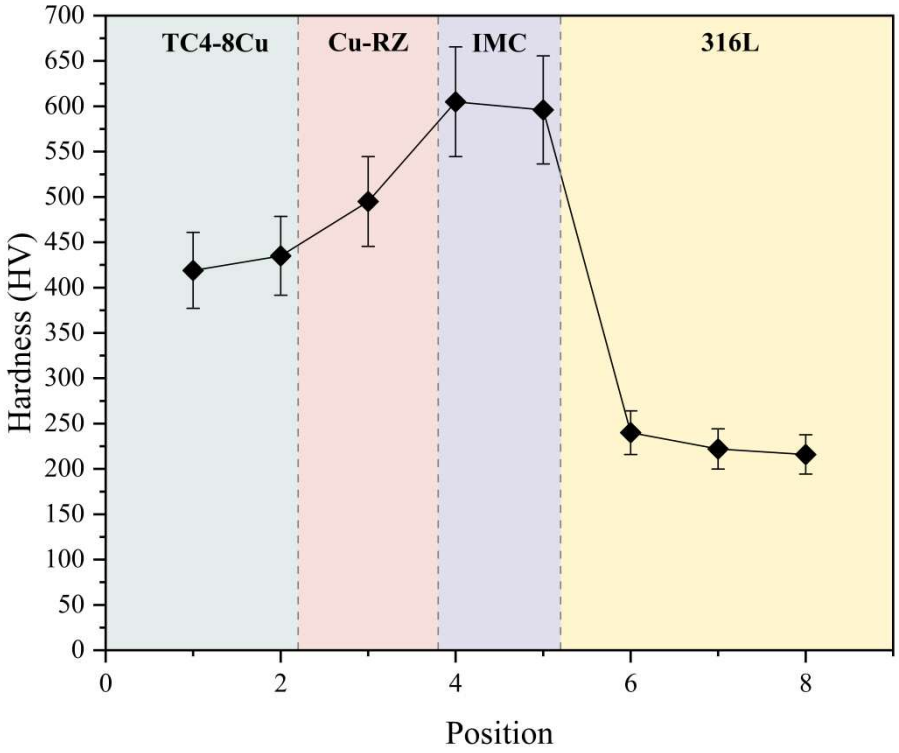

Fig. 9. Microhardness distribution across the TC4-8Cu/316 stainless steel interface

Table 6 Hardness values at the corresponding positions

Position	Zone	Hardness (HV)
1	TC4-8Cu	419
2	TC4-8Cu	435
3	Cu-rich zone	495
4	Intermetallic compound zone	605

5	Intermetallic compound zone	596
6	316L	240
7	316L	222
8	316L	216

Unlike pre-placed Cu foil interlayers, which may melt almost completely during welding and rely on residual unmelted Cu to block Ti-Fe contact [29], the Cu added to the TC4 powder is distributed throughout the titanium-side melt pool. This ensures that Cu is available at the interface to participate in the Ti-Cu reaction even after repeated thermal cycles. However, the Ti-Cu compound layer itself can become a fracture site in Cu-interlayer systems, as reported in electron beam welded Ti/Cu/Fe joints where fracture occurred at the interfacial layer containing TiCu and Ti-Cu-Fe [30, 31], In the present study, although the intermetallic compound zone exhibits the highest hardness, the room-temperature tensile failure initiates on the 316L side rather than at the interface. This suggests that the Cu-rich zone and Ti_2Cu compound zone are not the weakest link in the joint.

3.3 High-Temperature Tensile Properties

Fig. 10 shows the engineering stress-strain curves of the TC4-8Cu/316L bimetallic specimens under tensile testing at 350 °C **Fig. 11** shows the macroscopic fracture morphology, and Error! Unknown switch argument. lists the corresponding mechanical property data.

Unlike at room temperature, the fracture sequence of the specimens at 350 °C changed significantly, with the titanium side failing first, followed by load transfer to the steel side for continued bearing. Point A corresponds to the first-stage peak stress at high temperature, which is 618 MPa. After the titanium side first fractured, the stress rapidly decreased to point B, with a load-transfer stress of 76 MPa. Subsequently, the load was mainly borne by the 316L stainless steel side, and the stress recovered and reached 190 MPa at point D before fracture.

Combined with **Fig. 11**, the 316L side exhibits a more obvious necking stage. Meanwhile, compared with room temperature, the steel side exhibits a longer plastic deformation stage at 350 °C (**Fig. 10**), indicating that 316L stainless steel still maintains good plastic stability at this temperature. In contrast, the titanium side exhibits no obvious necking and fractures more abruptly, indicating that its plastic deformation capacity significantly decreases at this temperature. Therefore, the failure mode of the specimen at high temperature changes from steel side preferential fracture at room temperature to titanium side preferential fracture.

The reversal in fracture sequence arises mainly from the different high-temperature responses of the two alloys. At 350 °C the strength-ductility balance of the TC4-8Cu side deteriorates, lowering its load-bearing capacity and causing it to fail first. The 316L steel, by contrast, retains good ductility and continues to deform after the titanium side has fractured, continuing to undergo significant plastic deformation after titanium-side fracture [32, 33]. Meanwhile, interfacial elemental diffusion is further enhanced at high temperature, which may lead to a decrease in the interface's resistance to crack initiation. However, the introduction of Cu still

effectively suppresses the excessive growth of Fe-Ti brittle phases, so that high-temperature interfacial failure manifests as titanium-side preferential fracture rather than instantaneous brittle fracture of the entire interface. This demonstrates that the Cu-modified interface still possesses a certain degree of structural integrity and load-transfer capability at high temperature.

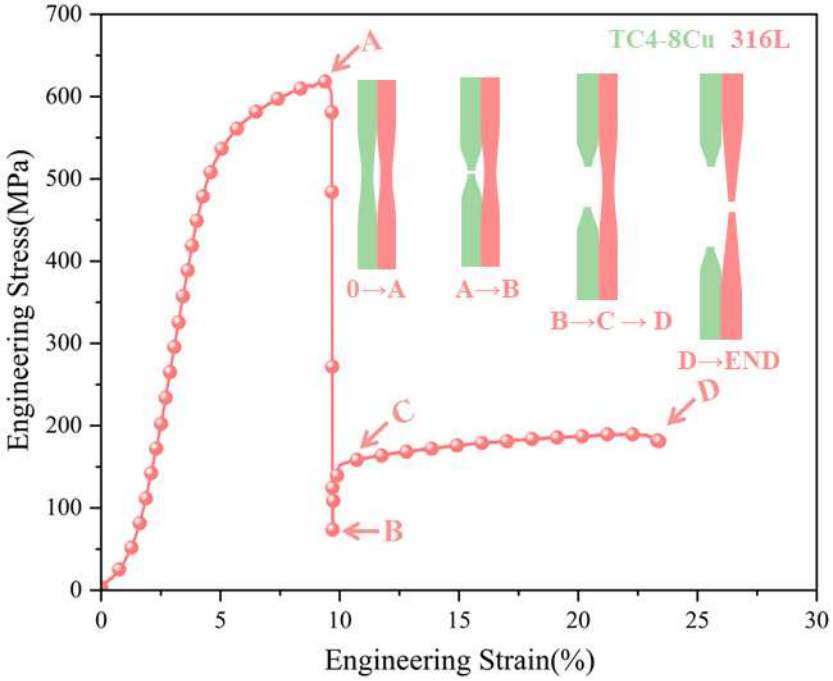

Fig. 10. Tensile stress-strain curves of TC4-8Cu/316 stainless steel at 350 °C

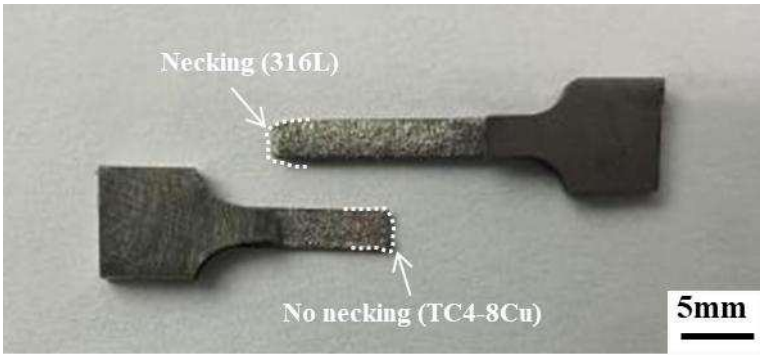

Fig. 11. High-temperature tensile fracture morphology of TC4-8Cu/316 stainless steel at 350 °C

Table 7 High-temperature mechanical property data at 350 °C

σ_1 (MPa)	σ_2 (MPa)	σ_b (MPa)	ε_1 (%)	δ (%)
618	76	190	9.7	23.1

σ_1=First-stage peak stress; σ_2=Load-transfer stress; σ_b=Ultimate tensile strength; ε_1=First-stage strain; δ=Total elongation at fracture.

4. Conclusions

(1) Effective metallurgical bonding was achieved between TC4-8Cu and 316L stainless steel by EB-PBF. The interface formed a multilayer transition structure consisting of a TC4-8Cu matrix, a Cu-rich reaction zone, an intermetallic compound zone, and a 316L matrix. The titanium side exhibits a lamellar α + β microstructure

with Cu mainly in solid solution, while the steel side is predominantly austenite with a small amount of δ-ferrite.

(2) Cu enriches in the near-interface region on the titanium side, forming a Cu-rich zone that limits direct Ti-Fe contact. The Ti and Fe concentration gradients at the interface are steep, indicating limited interdiffusion. Ti_2Cu is the main interfacial compound detected by XRD, while no obvious FeTi or Fe_2Ti diffraction peaks are observed. Cu preferentially reacts with Ti, consuming the Ti available for the Fe-Ti reaction and inhibiting the excessive growth of Fe-Ti brittle phases.

(3) The microhardness distribution across the interface is non-uniform, with the intermetallic compound zone exhibiting the highest hardness (596-605 HV). During room-temperature tension, the interface shows a distinct two-stage load-bearing behavior. The 316L side fails first at a first-stage peak stress of 482 MPa, after which the load is transferred to the titanium side, giving an ultimate tensile strength of 636 MPa.

(4) At 350 °C, the fracture sequence reverses: the TC4-8Cu side fails first at a first-stage peak stress of 618 MPa, and the load is subsequently transferred to the 316L side, which sustains approximately 190 MPa before final fracture. The interface still maintains load-transfer capability at high temperature, which is attributed to the regulation of the interfacial reaction path by Cu.

References

1. Luan Q, Liu J, Xia X et al (2025) Manufacturing methods, bonding mechanisms, and mechanical properties of titanium/steel clad plates. Front Mater Sci 19:250723. https://doi.org/10.1007/s11706-025-0723-2
2. Liang C Y, Lan S N, Wang Y S (2025) Review: high-performance dissimilar metal joining between titanium alloys and steel. J Mater Sci 60:13261-13293. https://doi.org/10.1007/s10853-025-11277-8
3. Wang C, Shang C, Liu Z et al (2020) Laser additive manufacturing of bimetallic structure from TC4 to IN718 via Ta/Cu multi-interlayer. Mater Res Express 7:126506. https://doi.org/10.1088/2053-1591/abce21
4. Gu C, Zeng S, Peng W et al (2023) Molecular dynamic simulation and experiment validation on the diffusion behavior of diffusion welded Fe-Ti by hot isostatic pressing process. Materials 16:5626. https://doi.org/10.3390/mal16165626
5. Chu Q, Xia T, Zhang L et al (2022) Interfacial microstructure and mechanical properties of titanium/steel dissimilar joining. Mater Lett 307:131069 https://doi.org/10.1016/j.matlet.2021.131069
6. Bai J, Liu C, Wu Y et al (2024) Research on the bonding performance and mechanism of hot-rolled Ti/steel clad plates based on surface state. J Mater Process Technol 333:118604. https://doi.org/10.1016/j.jmatprotec.2024.118604
7. Paul H, Morgiel J, Baudin T et al (2014) Characterization of explosive weld joints by TEM and SEM/EBSD. Arch Metall Mater 59:1129-1136. https://doi.org/10.2478/amm-2014-0197

8. Lei X L, Ding W H, Lu X X et al (2024) Interfacial modification of titanium/steel composites and its effect on the growth pattern of Fe-Ti compounds. Mater Today Commun 39:109289. https://doi.org/10.1016/j.mtcomm.2024.109289
9. Li P, Dong H, Xia Y et al (2018) Inhomogeneous interface structure and mechanical properties of rotary friction welded TC4 titanium alloy/316L stainless steel joints. J Manuf Process 33:54-63. https://doi.org/10.1016/j.jmapro.2018.05.001
10. Korzhyk V M, Khaskin V Y, Kvasnytskyi V V et al (2024) Preparing permanent joints of titanium alloys with steel (A review). Mater Sci 59:129-137. https://doi.org/10.1007/s11003-024-00753-2
11. Zhang L C, Liu Y, Li S et al (2018) Additive manufacturing of titanium alloys by electron beam melting: A review. Adv Eng Mater 20:1700842. https://doi.org/10.1002/adem.201700842
12. Galati M, Iuliano L (2018) A literature review of powder-based electron beam melting focusing on numerical simulations Additive Manufacturing 19:1-20. https://doi.org/10.1016/j.addma.2017.11.001
13. Osipovich K S, Kalashnikov K N, Vorontsov A V (2019) Alloying effect of Ti-6Al-4V on composite of 321 stainless steel fabricated by electron beam additive manufacturing. IOP Conf Ser Mater Sci Eng 537:022075.https://doi.org/10.1088/1757-899X/537/2/022075
14. Terentyev E V, Kozyrev K M, Borodavkina K T et al (2024) Obtaining of combined titanium-steel structures by electron beam freeform fabrication using niobium and copper interlayers. Int J Adv Manuf Technol 132:3519-3533. https://doi.org/10.1007/s00170-024-13556-1
15. Andreu A, Kim S, Kim I et al (2024) Processing challenges and delamination prevention methods in titanium-steel DED 3D printing. Intl J Precis Eng Manuf Green Technol 11:1663-1679. https://doi.org/10.1007/s40684-024-00598-9
16. Ma T J, Kang H, Wu Y Q et al (2004) Effects of rare earths on properties of Ti-Zr-Cu-Ni base brazing filler alloys.J.Rare Earth 22:214-217.
17. Mehta U, Yadav D R, Yadav S K et al (2025) Thermodynamic, surface and viscous properties of Cu-Fe-Ti alloys in liquid state based on exponential temperature-dependent interaction energy parameters. J Phase Equilib Diffus 46:267-278. https://doi.org/10.1007/s11669-025-01186-3
18. Sun K X, Liu Z, Wang F C et al (2025) Enhancement of strength-ductility of Ti-Cu alloy via uncontinuously ultrafine Ti_2Cu precipitation prepared by water-cooled laser-direct energy deposition. J Alloys Compd 1013:178580. https://doi.org/10.1016/j.jallcom.2025.178580
19. Wang T, Zhang B G, Chen G Q et al (2010) Electron beam welding of Ti-15-3 titanium alloy to 304 stainless steel with copper interlayer sheet. Trans Nonferrous Met Soc China 20:1829-1834. https://doi.org/10.1016/S1003-6326(09)60381-2
20. Ma Z, Liu D J, Xiao H T et al (2025) Effects of copper foil on the microstructure and mechanical properties of titanium/steel bimetallic sheet joints. Mater Today Commun 44:111917. https://doi.org/10.1016/j.mtcomm.2025.111917

21. Tomashchuk I, Sallamand P, Andrzejewski H et al (2011) The formation of intermetallics in dissimilar Ti6Al4V/copper/AISI 316 L electron beam and Nd:YAG laser joints. Intermetallics 19:1466-1473. https://doi.org/10.1016/j.intermet.2011.05.016
22. Zykova A P,Nikolaeva A V,Vorontsov A V et al (2023) Effect of copper content on grain structure evolution in additively manufactured Ti-6Al-4V alloy. Phys Mesomech 26:107-125. https://doi.org/10.1134/s1029959923020017
23. He Y, Ma Y, Zhang W et al (2022) Anisotropic tensile and fatigue properties of laser powder bed fusion Ti6Al4V under high temperature. Eng Fract Mech 276:108948. https://doi.org/10.1016/j.engfracmech.2022.108948
24. Wen T, Zhong Z H, Zhu S S et al (2025) Tensile mechanical behavior of additively manufactured 316L austenitic stainless steels in liquid lead-bismuth eutectic and in air. J Cent South Univ 32:2823-2840. https://doi.org/10.1007/s11771-025-6030-3
25. Guo H, Rao M, Zhang J et al (2023) Electromigration-enhanced Kirkendall effect of Cu/Ti direct diffusion welding by sparking plasma sintering. J Mater Process Technol 315:117933. https://doi.org/10.1016/j.jmatprotec.2023.117933
26. Ding H, Li M, Wen H et al (2025) Research on microstructure and mechanical properties of 316L stainless steel fabricated by coaxial electron beam wire feeding additive manufacturing. Mater Lett 399:138945. https://doi.org/10.1016/j.matlet.2025.138945
27. Bo H, Duarte L I, Zhu W J et al (2013) Experimental study and thermodynamic assessment of the Cu–Fe–Ti system. Calphad 40:24-33. https://doi.org/10.1016/j.calphad.2012.12.001
28. Huang L H, Ye C, Zhang B J et al (2025) First-principles study on structural, mechanical, and electronic properties of intermetallic compounds in titanium clad steel plates. Mater Today Commun 45:112272. https://doi.org/10.1016/j.mtcomm.2025.112272
29. Chen Y K, Zhou J P, Zhang Y et al (2021) Single-pass laser brazing of TC4 alloy and 304 stainless steel with Cu interlayer and Cu-Zn filler metal. Mater Lett 291:129357. https://doi.org/10.1016/j.matlet.2021.129357
30. Cheng Z, Wang Z, Bian Y F et al (2025) Oscillating laser welding of TC4-304SS dissimilar joints: Regulating microstructure and mechanical properties via Cu, Mo, and Nb interlayers. Materials 19:86. https://doi.org/10.3390/ma19010086
31. Hao X, Dong H, Xia Y et al (2019) Microstructure and mechanical properties of laser welded TC4 titanium alloy/304 stainless steel joint with (CoCrFeNi)100-xCux high-entropy alloy interlayer. J Alloys Compd 803:649-657. https://doi.org/10.1016/j.jallcom.2019.06.225
32. Thalavai Pandian K, Neikter M, Bahbou F et al (2022) Elevated-temperature tensile properties of low-temperature HIP-treated EBM-built Ti-6Al-4V. Materials 15:3624. https://doi.org/10.3390/ma15103624
33. Zhai W, Liu F, Wang Q et al (2024) Cryogenic and high temperature tensile properties of 316L steel additively manufactured by laser powder bed fusion. Mater Sci Eng A 900:146461. https://doi.org/10.1016/j.Msea.2024.146461